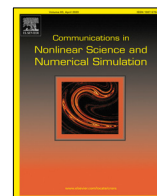




Contents lists available at ScienceDirect

# Communications in Nonlinear Science and Numerical Simulation

journal homepage: [www.elsevier.com/locate/cnsns](http://www.elsevier.com/locate/cnsns)

Research paper

## Chaos indicator and integrability conditions from geometrodynamics

A. Vergel<sup>a,b,1</sup>, J.C. Losada<sup>b,1</sup>, R.M. Benito<sup>b,1</sup>, F. Borondo<sup>a,c,\*</sup><sup>a</sup> Instituto de Ciencias Matemáticas (ICMAT), Cantoblanco, 28049 Madrid, Spain<sup>b</sup> Grupo de Sistemas Complejos, Escuela Técnica Superior de Ingeniería Agronómica, Alimentaria y de Biosistemas, Universidad Politécnica de Madrid, Avda. Puerta de Hierro 2-4, 28040 Madrid, Spain<sup>c</sup> Departamento de Química, Universidad Autónoma de Madrid, Cantoblanco, 28049 Madrid, Spain

### ARTICLE INFO

#### Article history:

Received 23 September 2022

Received in revised form 17 January 2023

Accepted 27 February 2023

Available online 2 March 2023

#### Keywords:

Chaos

Geometrodynamics

Riemannian metric

Weyl transformation

Catenary curve

### ABSTRACT

Stability and chaoticity in conservative Hamiltonian systems are analyzed using an indicator based on a generalization of the virtual work principle (VWP) for Riemannian manifolds. The geometrodynamical formalism obtained in this way is applied to define a mechanical manifold using the Jacobi metric, where the system trajectories are geodesics. The VWP for static mechanical equilibrium in Euclidean spaces is generalized and applied to trajectories in this manifold through geodesic equations derived from a Weyl transformation to this metric. We further interpret each trajectory of the system as a curve representing a non-stretchable string under tension derived from a potential function with constant length in this mechanical manifold, and analyze its stability through the fluctuation of an observable defined from the previous analysis. In this way, we can define a practical chaos indicator and find a sufficiency condition for a conservative dynamical system to have a regular dynamics. Several benchmark cases in two and three dimensions are presented as illustrations.

© 2023 The Author(s). Published by Elsevier B.V. This is an open access article under the CC BY-NC-ND license (<http://creativecommons.org/licenses/by-nc-nd/4.0/>).

## 1. Introduction

Extensive work has been published on many aspects of chaos theory in Hamiltonian systems. The search for efficient indicators of chaos for trajectories, as a tool to analyze the associated phase space structure, is an important task in this context. Accordingly, several such indicators have been proposed in the literature. Most of them, like the maximum Lyapunov exponents [1], small alignment index (SALI) [2,3], fast Lyapunov indicator (FLI) [4,5], mean exponential growth factor of nearby orbits (MEGNO) [6,7], or the frequency map analysis [8,9], are defined on the system phase space.

Another interesting alternative formalism is the use of geometrodynamics, which is defined in configuration space. In it, the system dynamics is recast into a Riemannian manifold, usually called mechanical manifold (MM), in such a way that the system trajectories are identified as the geodesics in it. Instability and chaos can be analyzed by studying indicators derived from the Jacobi-Levi-Civita (JLC) equation [10,11] in relation to the geodesic deviation vector. One example of such indicator is the stability geometrical indicator (SGI) introduced by us in Refs. [12,13]. Moreover, the same formalism

\* Corresponding author at: Departamento de Química, Universidad Autónoma de Madrid, Cantoblanco, 28049 Madrid, Spain.

E-mail addresses: [alberto.vergel.otero@upm.es](mailto:alberto.vergel.otero@upm.es) (A. Vergel), [juancarlos.losada@upm.es](mailto:juancarlos.losada@upm.es) (J.C. Losada), [rosamaria.benito@upm.es](mailto:rosamaria.benito@upm.es) (R.M. Benito), [f.borondo@uam.es](mailto:f.borondo@uam.es) (F. Borondo).

<sup>1</sup> All authors have contributed equal to this article.

have been used to find the location of conjugate points and compute Maslov indices of trajectories [14]. Also interesting in relation to the present work are Refs. [15–17] where non-Euclidean geometry is used to find reaction pathways.

Different metrics can be used in the geometrodynamical framework, for example those of Eisenhart [18], Finsler [19], and Jacobi [20–25], or others mainly based on conformal transformations [26,27]. In this context, the onset of chaos is caused in some systems by the negative curvature of the Hill's region border [12,28,29], or by the curvature generated by the mass matrix [12], among other reasons. However, it is commonly agreed that the onset of chaos depends in general on the dynamics, and it can be seen in the fluctuation of a suitable geometric observable, such as the scalar curvature of the manifold along the fiducial geodesic of reference. Indeed, the deviation of the JLC vector in two dimensional systems is governed by a harmonic oscillator equation where the frequency is replaced by the scalar curvature, this producing a parametric resonance, similarly to what happens, for example, in the Mathieu equation, which makes the trajectories to behave chaotically [30].

In this paper, we propose a new *catenary chaos indicator (CCI)* based on the analysis of the fluctuations of an observable suitably defined in the MM, based on an analogy existing between Mechanics and Statics, and we analyze its performance in the particular case of the two dimensional Hénon–Heiles Hamiltonian system [31] as an illustration. For other paradigmatic three dimensional Hamiltonian systems, we also find an analytical sufficiency stability condition. The idea, which dates back to the work of Johann Bernoulli [32], states that the problem of finding a particle trajectory connecting two points in configuration space can be formulated in purely equilibrium mechanical terms [33], as the minimum of the potential energy of a non-stretchable string under tension. Moreover, this analogy justifies that the mechanical principle of least action for a particle is equivalent to the static mechanical equilibrium (SME) of a flexible, non-stretchable string under the effect of a uniform gravitational field. Actually, in the geometrodynamical formalism it is possible to rewrite the differential equations for the hanging string (catenary curve) as the equations for the geodesics in the Riemannian manifold obtained from the Euclidean metric by a conformal transformation, being the tension  $T$  the corresponding conformal factor [34].

The goal of the present work is to study the stability of trajectories in a conservative dynamical system through the analysis of the static equilibrium for the corresponding trajectories, as if they were hanging flexible non-stretchable strings with fixed length in the previously mentioned MM. To this end we apply the Maupertuis variational principle which holds for isoenergetic asynchronous trajectories with fixed endpoints in configuration space endowed with the Jacobi metric. This process is carried out in three steps:

First, we geometrize the dynamics of our system following the geometrodynamical formalism, by building a Riemannian manifold where trajectories correspond to geodesics of the manifold. For this purpose, the MM derived from the Jacobi metric is used.

Second, in the MM previously determined, where now trajectories represent the geodesics in this underlying manifold MM, we use again the previous potential function  $V(q)$  as a scalar field at each point in order to obtain an action integral similar to the standard VWP for SME but considering now the MM as the underlying manifold instead of the Euclidean space. We show that applying this principle is equivalent to the computation of geodesics in the Riemannian manifold obtained as the Weyl transformation for the MM metric, thus deducing a new set of metric relations equivalent to the application of the VWP. Notice, that in the initial MM (before including the potential function) there are no real forces if energy is constant, the physical time  $t$  is then replaced by the arc length of the geodesics, and the velocity is unitary. Accordingly, the only forces are either fictitious or inertial (since they come from the Christoffel symbols [10,11] defined by the manifold). The fictitious forces can be eliminated locally using normal coordinates, this cancelling the Christoffel symbols. In these new coordinates, the geodesics equations correspond to straight lines in  $\mathbb{R}^n$ . Once the inertial forces have been eliminated locally and a potential function added, we can think (locally) about the same forces derived from the gradient of this potential function but without inertial forces. Interestingly enough, this way of proceeding is based on arguments [35] similar to those used by Fukui [36] in the context of chemical reactivity when defining the so-called intrinsic reaction coordinates curves in the search for reaction or minimum energy paths connecting reactants and products in the transition state theory [37]. Moreover, this interpretation is connected with the string method for computing minimum energy paths [38,39].

Finally, in the third step, we define an observable as the accumulated potential along the trajectory  $\gamma(s)$ , i.e.  $\int_{\gamma(s)} V ds$ , with constant length (as it is the case of the catenary string) in the MM, and we analyze its fluctuations as an indicator for stability and chaos, in the sense that larger fluctuations indicate more instability, while smaller fluctuations correspond to stable trajectories.

The organization of the paper is as follows. In Sections 2 and 3 the geometrodynamical formalism is introduced, first discussing the Jacobi metric and then recasting the VWP within this geometrical approach. In Section 4 we generalize the VWP to the MM, where trajectories are the geodesic lines in this space. In Sections 5 and 6 we first propose a practical chaos indicator definition (in 2D), and then we define an integrability criterion for conservative dynamic systems (in 3D). Section 7 is devoted to the analysis of some applications of this criterion and condition. The former is applied in Section 7.1 to the 2D Hénon–Heiles model, and the latter in Section 7.2 to a variety of well known integrable systems.

## 2. Geometric approach: The Jacobi metric

Let us consider a conservative system described by the Lagrangian defined in configuration space  $(q^i, \dot{q}^i)$  as (Einstein summation convention will be used throughout the paper)

$$\mathcal{L} = \mathcal{T} - V = \frac{1}{2} a_{ij}(\mathbf{q}) \dot{q}^i \dot{q}^j - V(\mathbf{q}), \quad (1)$$

where  $\dot{q}^i = dq^i/dt$ ,  $V(\mathbf{q})$  is the potential energy function, and  $a_{ij}(\mathbf{q})$  is the mass matrix. The associated natural motions are calculated as the extrema of the action integral

$$\delta \int \mathcal{L} dt = \delta \int \left[ \frac{1}{2} a_{ij}(\mathbf{q}) \dot{q}^i \dot{q}^j - V(\mathbf{q}) \right] dt = 0. \quad (2)$$

Alternatively, the system can be studied in phase space  $(q^i, p_j)$  through the identification  $p_j \leftrightarrow \partial \mathcal{L} / \partial \dot{q}^j$ , being  $p_j$  conjugate momenta. Then Hamilton principle of least action can be connected with the Maupertuis principle

$$\begin{aligned} \mathcal{A} &= \int_{\gamma(t)} p_i dq^i = \int_{\gamma(t)} \frac{\partial \mathcal{L}}{\partial \dot{q}^i} \dot{q}^i dt = \int_{\gamma(t)} 2\mathcal{T} dt, \\ \delta \mathcal{A} &= \delta \int_{\gamma(t)} 2\mathcal{T} dt = \delta \int_{\gamma(t)} \sqrt{2[E - V(\mathbf{q})] a_{ij}(\mathbf{q}) \dot{q}^i \dot{q}^j} dt = \delta \int_{\gamma(s)} \sqrt{\mathcal{G}_{ij}(\mathbf{q}) \dot{q}^i \dot{q}^j} ds = \delta \int_{\gamma(s)} ds = 0. \end{aligned} \quad (3)$$

That is, trajectories for Hamilton equations of motion correspond to geodesics in the Riemannian manifold MM with the metric  $\mathcal{G}_{ij}(\mathbf{q}) = 2[E - V(\mathbf{q})] a_{ij}(\mathbf{q})$ , being  $E$  the system total energy. From the previous results, we define the Jacobi metric in the corresponding Hill's region, i.e.  $M = \{\mathbf{q} = (q^1, \dots, q^N) / V(\mathbf{q}) < E\}$  as

$$\mathcal{G}_{ij}(\mathbf{q}) = 2[E - V(\mathbf{q})] a_{ij}(\mathbf{q}) dq^i \otimes dq^j, \quad (4)$$

being the mass matrix  $a_{ij}(\mathbf{q})$  positive defined and the arc length

$$ds = \sqrt{2[E - V(\mathbf{q})] a_{ij}(\mathbf{q}) \frac{dq^i}{dt} \frac{dq^j}{dt}} dt = \sqrt{2[E - V(\mathbf{q})]} dt. \quad (5)$$

Thus,

$$\mathcal{G}_{ij}(\mathbf{q}) = a_{ij}(\mathbf{q}) \frac{ds}{dt}. \quad (6)$$

## 3. Geometrodynamical approach to statics

In this section we study the catenary curve (see Fig. 1) as the most stable curve for a flexible, non-stretchable string in a generic forces field, showing that the stability analysis for this curve using the VWP from Statics can be recasted using the geometrodynamical theory. To this end we show the catenary curve is a geodesic line in a Riemannian manifold dowed with a metric tensor where the conformal factor is the tension along de curve.

The VWP asserts that for a mechanical system in static equilibrium the virtual work carried out by forces in a virtual displacement compatible with constraints is null. For applied forces derived from a potential, i.e.  $\mathbf{F} = -\nabla V$ , and holonomic constraints, the VWP can be written as follows

$$\delta \int V d\ell = 0. \quad (7)$$

with  $d\ell$  the arc length defined in the corresponding configuration space, commonly Euclidean.

We consider now the problem of the catenary curve, studied from a geometrodynamical perspective. Starting from generalized coordinates  $\{\mathbf{q}\}$ , the differential equations describing the curve for a flexible, non-stretchable string in a generic forces field can be written in general coordinates as [34]

$$\frac{dT_i}{ds} + \frac{\partial \mathcal{G}^{jk}}{\partial q^i} T_j T_k = \frac{\partial T}{\partial q^i}, \quad (8)$$

where  $T(\mathbf{q})$  is the tension of the string and  $\{\mathbf{e}_i(\mathbf{q})\}$  the associated canonical basis to  $\{\mathbf{q}\}$ , and

$$T_i = T \frac{dq^j}{ds} \mathbf{e}_j \cdot \mathbf{e}_i = T \frac{dq^j}{ds} \mathbf{e}_j \cdot \mathbf{e}_i = T \frac{dq^j}{ds} \mathcal{G}_{ji}, \quad (9)$$

where  $\cdot$  is the dot product,  $\mathcal{G}_{ji}$  the metric tensor components and  $\frac{dq^j}{ds}$  is the  $j$ th component of the unit tangent vector to the curve. Eq. (8) can be deduced from a geometrodynamical version [34], by making a conformal transformation to the Euclidean metric  $\delta_{ij}$  to obtain a Riemannian manifold with a new metric in coordinates given by

$$h_{ij} = T^2 \delta_{ij}. \quad (10)$$

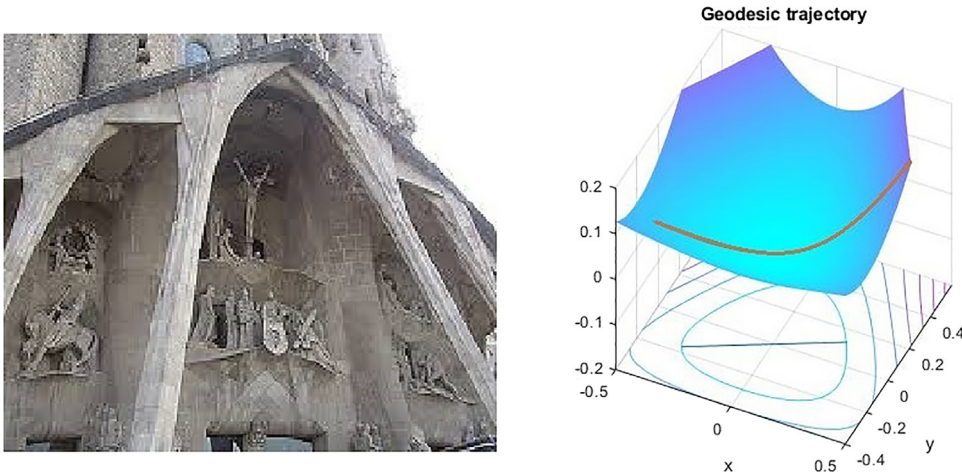


**Fig. 1.** (Left) Arches of Sagrada Família cathedral in Barcelona (Spain). Antoni Gaudí designed the shape of the archs such that the columns follow inverted catenary curves to ensure the structural mechanical stability [40]. (Right) An illustrative catenary curve for the Hénon–Heiles dynamical system.

In this case, the arc length for  $h_{ij}$  is  $d\bar{s} = \sqrt{T^2 \delta_{ij} dq^i dq^j} = T d\ell$ , being  $d\ell$  the Euclidean arc length. As pointed out before, trajectories are geodesics in this new metric, and the equations for the latter can be derived from the least action principle for the arc length

$$\delta \int d\bar{s} = 0. \quad (11)$$

In local coordinates these equations are

$$\begin{aligned} \frac{d^2 q^i}{d\bar{s}^2} + \Gamma_{jk}^i \frac{dq^j}{d\bar{s}} \frac{dq^k}{d\bar{s}} = \\ \frac{d^2 q^i}{d\bar{s}^2} + \frac{1}{2} h^{im} (\partial_j h_{mk} + \partial_k h_{mj} - \partial_m h_{jk}) \frac{dq^j}{d\bar{s}} \frac{dq^k}{d\bar{s}} = 0, \end{aligned} \quad (12)$$

where  $\Gamma_{jk}^i$  are the so-called Christoffel symbols [10,11] for the metric  $h_{ij}$ . Also, from the property of extrema (11) we obtain

$$\delta \int d\bar{s} = \delta \int \sqrt{h_{ij} dq^i dq^j} = \delta \int T \sqrt{\delta_{ij} dq^i dq^j} = \delta \int T d\ell \Big|_{T=V=\text{const}} = \delta \int V d\ell = 0, \quad (13)$$

with the constraint of constant length of the string. The last expression refers to the VWP (7) in  $\mathbb{R}^2$  for a force derived from a potential energy function obtained from the geometrodynamical version. We then conclude that equations for geodesics in the metric  $h_{ij}$  are equivalent to the equations for stable curves.

In the geometrodynamical version the property for geodesics (11) is used to derive trajectories verifying the VWP, this showing the fundamental character of the geometrodynamical formalism.

#### 4. Generalizing the virtual work principle

The idea, which dates back to the work of Johann Bernoulli [32], states that the problem of finding a particle trajectory connecting two points in configuration space can be formulated in purely equilibrium mechanical terms [33]. Our goal now is to study the stability for trajectories in conservative Hamiltonian dynamical systems using a principle similar to (7) applied to Statics.

To this end we use the geometrodynamical formalism, first defining a MM as indicated in Section 2 where trajectories are geodesics in this Riemannian manifold. Second, we define a potential function  $V(\mathbf{q})$  in this MM and show that the most stable trajectories for the Hamiltonian dynamical system are the geodesics of the metric obtained by a Weyl transformation applied to the Jacobi metric in MM. We start with the Jacobi metric previously defined in Section 2

$$\mathcal{G}_{\mu\nu}(\mathbf{q}) = 2[E - V(\mathbf{q})] a_{\mu\nu}(\mathbf{q}), \quad (14)$$

where the geodesic equations for  $\mathcal{G}_{\mu\nu}$  are

$$\frac{d^2 q^\mu}{ds^2} + \Gamma_{\lambda\nu}^\mu \frac{dq^\lambda}{ds} \frac{dq^\nu}{ds} = 0 \quad (15)$$

being  $\Gamma_{\lambda\nu}^{\mu}$  the Christoffel symbols and  $ds$  the arc length for the metric  $\mathcal{G}_{\mu\nu}$ . Now we carry out the conformal transformation, also known as the Weyl transformation,

$$\overline{\mathcal{G}}_{\mu\nu}(\mathbf{q}) = e^{2\Omega(\mathbf{q})} \mathcal{G}_{\mu\nu}(\mathbf{q}), \quad (16)$$

with arc length for this new metric

$$d\bar{s} = \sqrt{e^{2\Omega(\mathbf{q})} \mathcal{G}_{\mu\nu}(\mathbf{q}) \frac{dq^\mu}{ds} \frac{dq^\nu}{ds}} ds = e^{\Omega(\mathbf{q})} ds. \quad (17)$$

In order to obtain an action integral similar to the standard VWP for SME we make  $\Omega(\mathbf{q}) = \ln V(\mathbf{q})$  obtaining an expression equivalent to (7), and the variational principle as

$$\delta \int d\bar{s} = \delta \int e^{\Omega(\mathbf{q})} ds = \delta \int V(\mathbf{q}) ds = 0. \quad (18)$$

That is, the geodesics for the metric  $\overline{\mathcal{G}}_{\mu\nu}$  are those trajectories in the Jacobi metric which are extrema for the potential energy along them, which is equivalent to the VWP for forces derived from the potential energy function  $V$  but defined in the Riemannian manifold MM. The geodesics for the new metric (16) are then defined as

$$\frac{d^2 q^\mu}{d\bar{s}^2} + \overline{\Gamma}_{\lambda\nu}^{\mu} \frac{dq^\lambda}{d\bar{s}} \frac{dq^\nu}{d\bar{s}} = 0. \quad (19)$$

where

$$\overline{\Gamma}_{\lambda\nu}^{\mu} = \Gamma_{\lambda\nu}^{\mu} + \mathcal{G}^{\mu\sigma} (\mathcal{G}_{\sigma\nu} \partial_\lambda \Omega + \mathcal{G}_{\lambda\sigma} \partial_\nu \Omega - \mathcal{G}_{\lambda\nu} \partial_\sigma \Omega) \quad (20)$$

represents the new Christoffel symbols.

Moreover, taking into account that  $ds/d\bar{s} = e^{-\Omega(\mathbf{q})}$ , we have

$$\frac{d^2 q^\mu}{d\bar{s}^2} = \left( \frac{d^2 q^\mu}{ds^2} - \frac{dq^\mu}{ds} \frac{d\Omega}{ds} \right) e^{-2\Omega} \quad (21)$$

and Eq. (19) can be rewritten as

$$\frac{d^2 q^\mu}{ds^2} + \Gamma_{\lambda\nu}^{\mu} \frac{dq^\lambda}{ds} \frac{dq^\nu}{ds} + \frac{dq^\mu}{ds} \frac{d\Omega}{ds} - \partial^\mu \Omega = 0. \quad (22)$$

Considering now only trajectories which are geodesics for the Jacobi metric  $\mathcal{G}_{\mu\nu}$ , the two first terms in the l.h.s. of Eq. (22) cancel out, so that it further simplifies to

$$\frac{dq^\mu}{ds} \frac{d\Omega}{ds} - \partial^\mu \Omega = \frac{dq^\mu}{ds} \left( \partial_\alpha \Omega \frac{dq^\alpha}{ds} \right) - \partial^\mu \Omega = 0. \quad (23)$$

Finally, changing from the length parameter  $s$  to the physical time  $t$ , using the relationship  $ds = 2[E - V(\mathbf{q})] dt = 2W dt \rightarrow dt/ds = 1/(2W)$ , Eq. (23) results in

$$\frac{dq^\mu}{dt} \left( \partial_\alpha \Omega \frac{dq^\alpha}{dt} \right) = 4W^2 \partial^\mu \Omega. \quad (24)$$

For the case of 2D Hamiltonian conservative systems, this expression is written explicitly as

$$\begin{aligned} \frac{dq^1}{dt} \left( \partial_1 \Omega \frac{dq^1}{dt} + \partial_2 \Omega \frac{dq^2}{dt} \right) &= 4W^2 \mathcal{G}^{11} \partial_1 \Omega \\ \frac{dq^2}{dt} \left( \partial_1 \Omega \frac{dq^1}{dt} + \partial_2 \Omega \frac{dq^2}{dt} \right) &= 4W^2 \mathcal{G}^{22} \partial_2 \Omega. \end{aligned} \quad (25)$$

The solution of these equations is given implicitly by  $\mathcal{G}^{22} \partial_2 \Omega (dq^1/dt) - \mathcal{G}^{11} \partial_1 \Omega (dq^2/dt) = 0$ , or equivalently by

$$a^{22} \partial_2 \Omega \frac{dq^1}{dt} - a^{11} \partial_1 \Omega \frac{dq^2}{dt} = 0, \quad (26)$$

since the Jacobi metric  $\mathcal{G}_{\mu\nu}(\mathbf{q})$  is a conformal transformation. In the case that  $a_{ij}(\mathbf{x}) = \delta_{ij}$  the above expression can be interpreted geometrically as

$$\nabla \Omega \cdot \dot{\gamma}^\perp = 0 \Rightarrow \nabla \Omega \parallel \dot{\gamma}, \quad (27)$$

where  $\dot{\gamma} = (dq^1/dt)\mathbf{e}_1 + (dq^2/dt)\mathbf{e}_2$ , the same stability condition holds for the case  $\Omega(\mathbf{q}) = \ln V(\mathbf{q})$ .

This expression can be extended to 3D in the following way

$$\begin{aligned}\frac{dq^1}{dt} \left( \partial_1 \Omega \frac{dq^1}{dt} + \partial_2 \Omega \frac{dq^2}{dt} + \partial_3 \Omega \frac{dq^3}{dt} \right) &= 4W^2 \mathcal{G}^{11} \partial_1 \Omega \\ \frac{dq^2}{dt} \left( \partial_1 \Omega \frac{dq^1}{dt} + \partial_2 \Omega \frac{dq^2}{dt} + \partial_3 \Omega \frac{dq^3}{dt} \right) &= 4W^2 \mathcal{G}^{22} \partial_2 \Omega \\ \frac{dq^3}{dt} \left( \partial_1 \Omega \frac{dq^1}{dt} + \partial_2 \Omega \frac{dq^2}{dt} + \partial_3 \Omega \frac{dq^3}{dt} \right) &= 4W^2 \mathcal{G}^{33} \partial_3 \Omega\end{aligned}\quad (28)$$

can be reduced to

$$\begin{aligned}\mathcal{G}^{11} \partial_1 \Omega \frac{dq^2}{dt} - \mathcal{G}^{22} \partial_2 \Omega \frac{dq^1}{dt} &= 0 \\ \mathcal{G}^{22} \partial_2 \Omega \frac{dq^3}{dt} - \mathcal{G}^{33} \partial_3 \Omega \frac{dq^2}{dt} &= 0 \\ \mathcal{G}^{11} \partial_1 \Omega \frac{dq^3}{dt} - \mathcal{G}^{33} \partial_3 \Omega \frac{dq^1}{dt} &= 0\end{aligned}\quad (29)$$

or alternatively to the same expressions just changing  $\mathcal{G}^{ij}$  by  $a^{ij}$ .

Again, for  $a_{ij} = \delta_{ij}$  and  $\Omega(\mathbf{q}) = \ln V(\mathbf{q})$ , a geometrical interpretation of this solution analogous to Eq. (29) is obtained, except that now the usual external product in  $\mathbb{R}^3$  substitutes the dot product in  $\mathbb{R}^2$  i.e.  $|\nabla \Omega \wedge \dot{\gamma}^\perp| = 0$ . The solutions do not depend on the conformal metric,  $\mathcal{G}_{ij}(\mathbf{q})$ , but on the initial one,  $a_{ij}(\mathbf{q})$ .

More interestingly, in the previous case  $\Omega(\mathbf{q}) = \ln V(\mathbf{q})$  with  $a^{ij} = \delta^{ij}$  we can add the three expressions in Eq. (29) and define a new scalar variable,  $I$ , from which a necessary condition for regularity is obtained in the case of catenary trajectories, i.e.

$$I = \left( \frac{\partial V}{\partial q^3} - \frac{\partial V}{\partial q^2} \right) \frac{dq^1}{dt} + \left( \frac{\partial V}{\partial q^1} - \frac{\partial V}{\partial q^3} \right) \frac{dq^2}{dt} + \left( \frac{\partial V}{\partial q^2} - \frac{\partial V}{\partial q^1} \right) \frac{dq^3}{dt} = 0. \quad (30)$$

We call Eqs. (26) and (30) the *catenary regularity conditions* for trajectories in 2D and 3D, respectively.

## 5. Defining the chaos indicator

The aim of the present section is to define a new chaos indicator based on the properties of the catenary trajectories.

We start by assuming that such an indicator must depend on the dynamics of the system, i.e. on the history of the trajectory. Taking this and the results from the previous section into account, we propose to define an adequate observable depending on expression (26) along the trajectory determining its level of stability. Suitable magnitudes are  $\nabla \Omega \cdot \dot{\gamma}^\perp$  for 2D systems, and (30) in the case 3D with the metric tensor  $a_{ij}(\mathbf{q}) = \delta_{ij}$ , and  $\Omega(\mathbf{q}) = \ln V(\mathbf{q})$ . Following Eq. (26), we define for 2D systems the observable as

$$\mathcal{O}(\mathbf{q}(t)) = \frac{1}{|\nabla V| \|\dot{\gamma}(t)\|} \left( a^{22} \partial_2 V \frac{dq^1}{dt} - a^{11} \partial_1 V \frac{dq^2}{dt} \right), \quad (31)$$

which measures the mutual projection of the normalized vectors  $\nabla V$  and  $\dot{\gamma}^\perp$  along the trajectory calculated using the metric tensor  $a^{ij}$ , i.e. its degree of alignment. We then define a new chaos indicator, namely the catenary chaos indicator (CCI)  $\sigma_\gamma$  as the mean squared error of  $\mathcal{O}$  along the trajectory  $\gamma$ , i.e.

$$\sigma_\gamma(t) = \sqrt{\frac{\langle (\mathcal{O} - \langle \mathcal{O} \rangle_t)^2 \rangle}{t}}, \quad (32)$$

with  $\langle \mathcal{O} \rangle_\tau = \frac{1}{\tau} \int_0^\tau \mathcal{O}(\xi) d\xi$ , and

$$\langle (\mathcal{O} - \langle \mathcal{O} \rangle_t)^2 \rangle = \int_0^t (\mathcal{O}(\tau) - \langle \mathcal{O} \rangle_\tau)^2 d\tau, \quad (33)$$

for a constant value  $L$  of the arc length  $s = 2 \int_0^t [E - V(\mathbf{q}(t))] dt = L$ . In Eq. (32),  $\langle \dots \rangle_t$  indicates time average over the time lapse  $[0, t]$ , and it is worth noting that each trajectory needs a different physical time  $t$  interval to reach the length  $L$ .

The most stable trajectories are expected to correspond to null values for the observable  $\mathcal{O}$ , so that analyzing this fluctuation the stability level for the trajectory  $\gamma$  can be inferred, as will be illustrated in Section 7.

## 6. Integrability conditions in 3D

The aim of this section is to present a sufficiency condition for conservative dynamical systems to be integrable, based again in the local stability of the catenary trajectories, setting the analogy with David Gregory proposition in Structural Mechanics about archs: 'An arch of any form can only be in equilibrium if we can draw a catenary curve which passes



through it' (see Fig. 1). Accordingly the catenary curve is a local stabilizer, hence if the configuration space is fulfilled with catenary curves the dynamics is regular. The idea is to study the possibility of densely foliating the configuration space with catenary submanifolds, i.e. submanifolds generated by catenary trajectories fulfilling the condition (30) and, when possible, deducing the global regularity.

As derived in Section 4 we have that for a catenary trajectory there exist a scalar magnitude  $I$  which nullifies along it. And, moreover, with the corresponding stability neighborhood of these trajectories in systems with mixed dynamics, as shown in case 2D with the trajectories in Fig. 3 panels (a) and (b) corresponding with the two elliptic points in Fig. 2 panel (a).

We need now to generalize Eq. (30) to the whole space  $\mathbb{R}^3$  finding out two dimensional submanifolds generated by catenary trajectories. This will allow to assert or not the general regular dynamics and integrability.

Geometrically, if Eq. (30) is fulfilled there exist a submanifold immersed in  $\mathbb{R}^3$ , the *catenary submanifold*, defined as  $U(\mathbf{q}) = k$ , where for  $a_{ij} = \delta_{ij}$  we have that  $d\mathbf{q}/dt \equiv \mathbf{p} = (p_1, p_2, p_3) \in T_{\mathbf{q}}U(\mathbf{q})$  and the submanifold normal vector  $\nabla U(\mathbf{q}) = \left( \frac{\partial V}{\partial q^3} - \frac{\partial V}{\partial q^2}, \frac{\partial V}{\partial q^2} - \frac{\partial V}{\partial q^1}, \frac{\partial V}{\partial q^1} - \frac{\partial V}{\partial q^3} \right)$  is orthogonal to  $\mathbf{p}$ . Moreover, we also have the identity

$$\nabla V(\mathbf{q}) \cdot \nabla U(\mathbf{q}) \equiv 0 \quad (34)$$

where the dot represents the natural dot product, which indicates that the forces are tangent to the submanifold  $U(\mathbf{q}) = k$ , so that any trajectory with initial conditions in this submanifold is totally confined in it. The existence of such submanifolds for different values of  $k$ , makes the dynamics for the catenary trajectories be laminar, and then  $\mathbb{R}^3$  is foliated by catenary submanifolds, which are locally regular.

In order to show analytically the existence of submanifolds  $U(\mathbf{q}) = k$  for the case of a particular Hamiltonian, the first order partial differential equation (30) equivalent to the *Pfaffian* equation in 3D

$$\omega \equiv P(\mathbf{q})dq^1 + Q(\mathbf{q})dq^2 + R(\mathbf{q})dq^3 = 0, \quad (35)$$

has to be solved, where  $\mathbf{q} \in D \subset \mathbb{R}^3$  and  $\omega$  a differential 1-form with  $\mathbf{q} = (q^1, q^2, q^3)$  and  $P(\mathbf{q}), Q(\mathbf{q}), R(\mathbf{q}) \in C^1(D)$ . Frobenius theorem asserts that the necessary and sufficient condition for complete integrability of (35) is

$$d\omega \wedge \omega \equiv 0, \quad (36)$$

in the three dimensional case it translates into

$$P \left( \frac{\partial Q}{\partial q^3} - \frac{\partial R}{\partial q^2} \right) + Q \left( \frac{\partial R}{\partial q^1} - \frac{\partial P}{\partial q^3} \right) + R \left( \frac{\partial P}{\partial q^2} - \frac{\partial Q}{\partial q^1} \right) = 0, \quad (37)$$

or in vectorial language to  $\text{curl} \vec{F} \cdot \vec{F} = 0$  with  $\vec{F} = (P(\mathbf{q}), Q(\mathbf{q}), R(\mathbf{q}))$ . In this case, a function  $\mu(\mathbf{q}) \neq 0$  can be found as integrating factor so that a smooth function  $U(\mathbf{q})$  exists, and

$$dU \equiv \mu(P(\mathbf{q})dq^1 + Q(\mathbf{q})dq^2 + R(\mathbf{q})dq^3) = 0. \quad (38)$$

Expressed in coordinates  $\{q^i\}$ , this equation along a trajectory corresponds to

$$\frac{dU(q^i(t))}{dt} = \mu \left( P(\mathbf{q}) \frac{dq^1}{dt} + Q(\mathbf{q}) \frac{dq^2}{dt} + R(\mathbf{q}) \frac{dq^3}{dt} \right) = 0 \quad (39)$$

and for the initial conditions  $\mathbf{q}_0 = (q_0^1, q_0^2, q_0^3)$  there is only one real value  $k$  for which  $U(\mathbf{q}_0) = k$ . Taking into account this identity, the trajectory with initial conditions  $(q_0^i) \in U(\mathbf{q}) = k$  and  $dq^i/dt \in T_{\mathbf{q}}U(\mathbf{q})$  is always confined to the manifold  $U(\mathbf{q}) = k$  so that we can reduce the 3D dynamics to a 2D one. This assertion restricts the system chaoticity because any trajectory with the previous initial conditions cannot scape from this locally steady catenary submanifold, this preventing it to reach different regions of the phase space. From this analysis we make the following integrability assertion: A Hamiltonian mechanical system with Hamiltonian function expressed in canonical coordinates  $(\mathbf{q}, \mathbf{p}) = (q^1, q^2, q^3, p_1, p_2, p_3)$  as

$$H(\mathbf{q}, \mathbf{p}) = \frac{1}{2} \sum_{i=1}^3 (p_i)^2 + V(\mathbf{q}) \quad (40)$$

and considering the vector field  $P(\mathbf{q})\partial_{q^1} + Q(\mathbf{q})\partial_{q^2} + R(\mathbf{q})\partial_{q^3}$  in  $\mathbb{R}^3$  with

$$\begin{aligned} P(\mathbf{q}) &= \frac{\partial V}{\partial q^3} - \frac{\partial V}{\partial q^2} \\ Q(\mathbf{q}) &= \frac{\partial V}{\partial q^1} - \frac{\partial V}{\partial q^3} \\ R(\mathbf{q}) &= \frac{\partial V}{\partial q^2} - \frac{\partial V}{\partial q^1} \end{aligned} \quad (41)$$

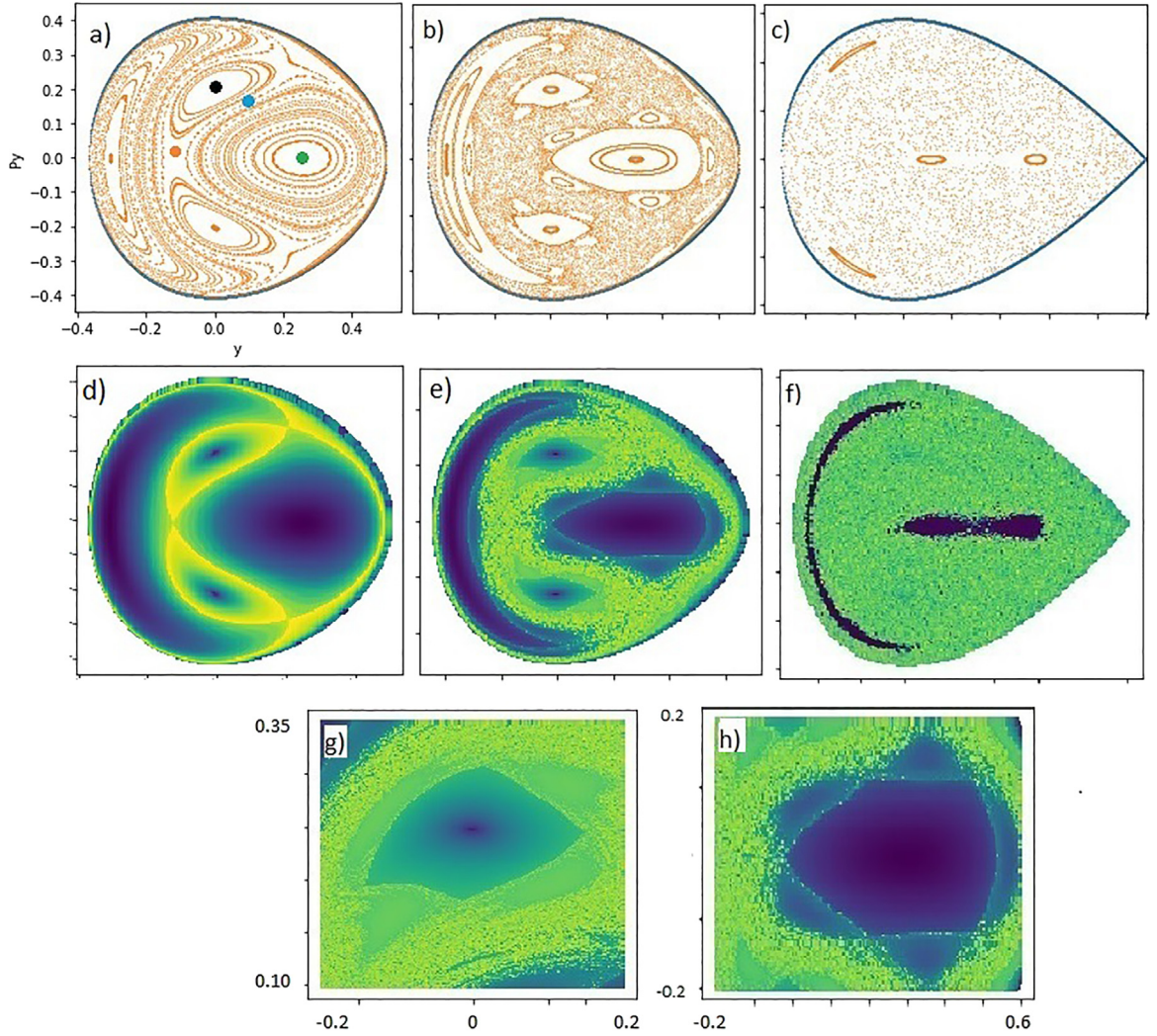


**Fig. 2.** (a)–(c) Poincaré surface of section  $x = 0$  and  $P_x < 0$ , and (d)–(f) the chaos indicator  $\sigma_\gamma$  defined in Eq. (32) and computed for a total geodesic length  $s = 100$  for the Hénon–Heiles system at  $E = 1/12$  (a) and (d),  $1/8$  (b) and (e), and  $1/6$  (c) and (f). The positions of four particular trajectories for  $E = 1/12$ , located at  $(y, P_y) = (0, 0.2040)$  (black),  $(0.2545, 0)$  (green),  $(-0.1200, 0.0045)$  (red), and  $(0.1000, 0.1850)$ , which will be further analyzed in Fig. 3, are indicated with colored points. Blown ups of  $\sigma_\gamma$  in two resonance zones for  $E = 1/8$  are presented in panels (g) and (h).

if condition

$$P \left( \frac{\partial Q}{\partial q^3} - \frac{\partial R}{\partial q^2} \right) + Q \left( \frac{\partial R}{\partial q^1} - \frac{\partial P}{\partial q^3} \right) + R \left( \frac{\partial P}{\partial q^2} - \frac{\partial Q}{\partial q^1} \right) \equiv 0 \quad (42)$$

is fulfilled identically, then there exist catenary submanifolds, locally regular and densely foliating  $\mathbb{R}^3$ , where catenary trajectories are confined totally in leaves  $U(\mathbf{q}) = k$ , i.e. its dynamics is laminar with  $p_1(t)P(\mathbf{q}(t)) + p_2(t)Q(\mathbf{q}(t)) + p_3(t)R(\mathbf{q}(t)) = 0$ , this inducing the whole dynamics to be regular.

## 7. Numerical results

### 7.1. Chaos criterion in the 2D Hénon–Heiles system

In this subsection we apply our CCI to the paradigmatic Hénon–Heiles Hamiltonian [31], originally proposed to study the motion of stars around a galactic center. It consists of two oscillators coupled with a cubic term

$$H(x, y, P_x, P_y) = \frac{1}{2} (P_x^2 + P_y^2 + x^2 + y^2) + x^2 y - \frac{1}{3} y^3. \quad (43)$$



The potential function has a  $C_{3v}$  (triangular) symmetry, and bounds the motion up to an energy of  $E \leq 1/6$ . Above this value, the particle can escape through the three exit channels existing along the polar angles  $\pi/2$ ,  $7\pi/6$ , and  $11\pi/6$ , at which three saddles exist located at  $(x, y) = (0, 1), (\pm\sqrt{3}/2, -1/2)$ .

The corresponding dynamics can be adequately followed by numerically propagating trajectories with randomly chosen initial conditions in phase space at constant energy, and extracting dynamical information from them by computing Poincaré surfaces of section (PSOS) using a suitable sectioning plane, which in our case is taken at  $x = 0$  and  $P_x < 0$ . This allows to distinguish the regions of phase space with regular motion from those in which it is chaotic. Also, periodic orbits exist which leave a characteristic imprint in the PSOS, it consisting of an integer number of fixed points (corresponding to the order of the resonance) with a visible pattern of islands around them and an stochastic band of chaos in between, as dictated by the well known Poincaré–Birkhoff theorem [41].

Some PSOS results are presented in Fig. 2(a), (b) and (c) for  $E = 1/12, 1/8$  and  $1/6$ , respectively. As can be seen, at  $E = 1/12$  all motion is regular taking place in invariant tori, and seven fixed points corresponding to different existing POs [42] can be seen. Four of them, located at  $(-0.3123, 0), (0, \pm 0.2040)$  and  $(0.2545, 0)$  are stable, while the other three, located at  $(-0.120, 0)$  and  $(0.208, \pm 0.275)$ , are unstable. They correspond respectively to  $\Pi_7, \Pi_{2,3}$ , and  $\Pi_8, \Pi_{4,5,6}$  in the standard nonlinear local modes of Ref. [42]. Among them, we have considered four representative orbits corresponding to the colored points marked in Fig. 2(a) to be studied later. As energy increases, for example to  $E = 1/8$  in Fig. 2(b), more and more invariant tori are destroyed as dictated by the Kolmogorov, Arnold and Moser (KAM) theorem [43], the bands of stochasticity connecting the unstable fixed point grow, and chaos spread in phase space. Finally, at energies close and above the escape limit, for example  $E = 1/6$  in Fig. 2(c), almost all the dynamics is chaotic, and very few traces of regularity are visible.

The corresponding results obtained with our CCI  $\sigma_\gamma(s)$ , defined in Eq. (32) and computed for a total geodesic length of  $s = 100$ , are shown with a color scale in Figs. 2 (d), (e), and (f), for the same energy values as before. The way in which these color map are made is the following. We first numerically propagate trajectories with the same randomly chosen initial conditions and energies previously used to compute the PSOS. The CCI indicator is computed next along each one of them for a fixed total geodesics length. The values for the indicator are then transformed to colors at each point, i.e. initial condition, according to its magnitude. Notice that no color scales have been included in the plots. This is due to the fact that the absolute value of the CCI has no comparative meaning since they varied with the total energy at which they are computed, having them being renormalized in our presentation.

Here, darker colors indicate the position of the more regular trajectories, while the lighter indicate irregularity and chaos. Starting with the lowest energy  $E = 1/12$ , we see in panel (d) that we have two kind of regions, indicating the position of the elliptic islands, i.e. regularity, and the bands of stochasticity, respectively, all in agreement with the previously commented PSOS results of panel (a). More interestingly, our CCI  $\sigma_\gamma$  shows different color tones around the two elliptic fixed points with  $y = 0$  and  $p_y = 0$ , this indicating that it is able to detect a different degree of stability (higher for the latter and lower for the former) among them. The results for the higher energy  $E = 1/8$  [panel (e)] have essentially the same overall structure, but clearly show the expected increase in chaoticity due to the destruction of invariant tori. Also, the islands around island structure is better developed, and a conspicuous 1:5 resonance is visible around the fixed point at  $(0.2545, 0)$ . Again our chaos indicator shows a stability difference among regular regions. This effect is further studied in the blown up presented in panels (g) and (h), the former showing the region around the stable elliptic fixed points with  $y = 0$ , and the latter the other one located on the  $P_y = 0$  line. Notice that this also explains, in a very easy way, why some stability regions around the elliptic points disappears earlier than others as  $E$  increases. Finally, Fig. 2(f) show the results corresponding to the highest energy considered  $E = 1/6$ . At this value, almost all invariant tori are broken, although some tiny islands of high (very dark color) regularity, centered on the  $P_y = 0$  axis, are visible.

To finish this subsection, we will next analyze the performance of our CCI when applied to specific trajectories. For this purpose we choose four representative orbits for  $E = 1/12$  corresponding to the colored points marked in Fig. 2(a). The first two (black and green) correspond to stable periodic orbits, the third one (red) corresponds to unstable periodic orbit complementary (in the sense of the Poincaré–Birkhoff theorem [41]) to the former one (black), and the fourth one (blue) is in the associated stochasticity band, where the motion is chaotic. The corresponding orbits in the configuration space  $(x, y)$  are shown in Fig. 3(a)–(d), and the associated evolution of our chaos indicator *versus* the arc-length  $s$  in panel (e). Several comments are in order. In the first place, in all cases a fast converge of  $\sigma_\gamma$  with  $s$  is found. Second, our chaos indicator correctly separates the stable/regular from the unstable/chaotic trajectories. Indeed, the value of  $\sigma_\gamma$  is smaller for the first two trajectories (black and green) and greater for the other two (red and blue). Third,  $\sigma_\gamma$  assigns the same value to both irregular trajectories, since they are in the same stochasticity band. Fourth, our indicator assign different values to the two stable trajectories considered indicating different degrees of stability for the two associated phase space regular regions. Our results can be compared to other similar calculations. Indeed, in Fig. 9 of Ref. [2]. Skokos et al. presented SALI maps computed in the same conditions that ours. As can be seen, our results are totally equivalent to theirs, and the same conclusions (at least qualitatively) regarding regular and chaotic regions in the Hénon–Heiles system can be extracted from both works.

## 7.2. Integrability conditions in 3D

In Section 6 a sufficiency condition (42) for a conservative dynamical system with Hamiltonian function of type (40) to be integrable was deduced without making any reference to first integrals. In this subsection we will apply

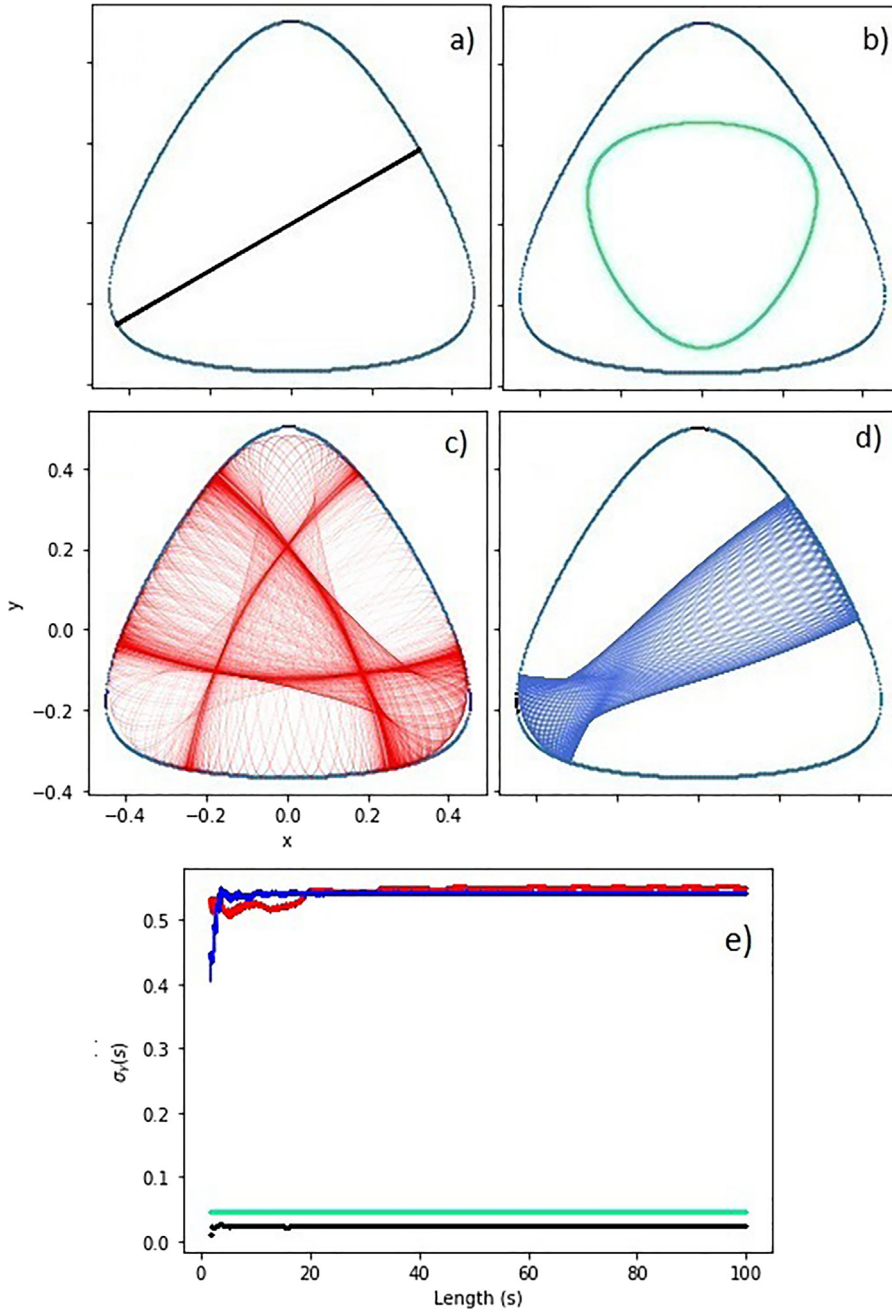


**Fig. 3.** Regular trajectories for  $E = 1/12$  (a) (black), (b) (green), and chaotic (c) (red), (d) (blue) corresponding to the initial conditions marked in Fig. 2(a). (e) Corresponding evolution of the chaos indicator  $\sigma_y$  using the same color code.

that integrability condition to non-trivial conservative Hamiltonian systems of the same form. We consider, as well, the integrability for general three dimensional Hamiltonians with central or exponential potential functions in the same way, i.e. without making reference to first integrals.

An important remark to make here is the following. Since the integrability condition (42) is a sufficient condition, there may be cases of integrable systems with a generic potential function which do not fulfill the previous condition. Some examples of this will be presented.

### 7.2.1. Systems with 3D central potentials

Let us first consider the case of systems subject to central potentials. In cartesian coordinates these systems are described with the general Hamiltonian function

$$H = \frac{1}{2} (p_1^2 + p_2^2 + p_3^2) + V(\mathbf{r}), \quad (44)$$

being  $V(\mathbf{r})$  a general function depending only on the Euclidean distance  $\mathbf{r} = [(q^1)^2 + (q^2)^2 + (q^3)^2]^{\frac{1}{2}}$ . From expression (41) it is easy to show that

$$\begin{aligned} P(\mathbf{q}) &= \frac{\partial V}{\partial q^3} - \frac{\partial V}{\partial q^2} = \frac{\partial V}{\partial \mathbf{r}} \frac{1}{\mathbf{r}} (q^3 - q^2), \\ Q(\mathbf{q}) &= \frac{\partial V}{\partial q^1} - \frac{\partial V}{\partial q^3} = \frac{\partial V}{\partial \mathbf{r}} \frac{1}{\mathbf{r}} (q^1 - q^3), \\ R(\mathbf{q}) &= \frac{\partial V}{\partial q^2} - \frac{\partial V}{\partial q^1} = \frac{\partial V}{\partial \mathbf{r}} \frac{1}{\mathbf{r}} (q^2 - q^1). \end{aligned} \quad (45)$$

The vector field  $\vec{F} = (P(\mathbf{q}), Q(\mathbf{q}), R(\mathbf{q}))$  is perpendicular to the catenary submanifold  $U(\mathbf{q})$ , i.e.  $\vec{F} = \nabla U(\mathbf{q})$ , and then fulfills the integrability condition (42)  $\text{curl} \vec{F} \cdot \vec{F} = 0$ .

An example of this kind of systems is the Kepler problem

$$V(\mathbf{r}) = -\frac{1}{\mathbf{r}} = -\frac{1}{\sqrt{(q^1)^2 + (q^2)^2 + (q^3)^2}} \quad (46)$$

for which

$$\begin{aligned} P(\mathbf{q}) &= \frac{\partial V}{\partial q^3} - \frac{\partial V}{\partial q^2} = \frac{q^3 - q^2}{((q^1)^2 + (q^2)^2 + (q^3)^2)^{\frac{3}{2}}}, \\ Q(\mathbf{q}) &= \frac{\partial V}{\partial q^1} - \frac{\partial V}{\partial q^3} = \frac{q^1 - q^3}{((q^1)^2 + (q^2)^2 + (q^3)^2)^{\frac{3}{2}}}, \\ R(\mathbf{q}) &= \frac{\partial V}{\partial q^2} - \frac{\partial V}{\partial q^1} = \frac{q^2 - q^1}{((q^1)^2 + (q^2)^2 + (q^3)^2)^{\frac{3}{2}}}, \end{aligned} \quad (47)$$

The corresponding (normalized) vector field  $\vec{F} = (P(\mathbf{q}), Q(\mathbf{q}), R(\mathbf{q}))$  is shown in Fig. 4, where we see that the flow of the field corresponds to circumferences described in a counterclockwise fashion. The location of the corresponding rotation axis is appreciated in the plot, and the catenary submanifolds are geometrically defined as the bundle of planes perpendicular to  $\vec{F}$  passing through this axis.

### 7.2.2. 3D Toda molecule and lattice

Let us consider now the generic potential functions

$$V_j(\mathbf{q}) = e^{\alpha q^{j+1} + \beta q^j} \quad (48)$$

which fulfills the integrability condition (42), and so it also does it potentials of the form  $V = \sum_j V_j$ . In particular, we consider the Toda Molecule, i.e. a system consisting of 3-mass points in a line with coordinates  $q^1, q^2, q^3$  described by Hamiltonian

$$H = \frac{1}{2} (p_1^2 + p_2^2 + p_3^2) + e^{q^1 - q^2} + e^{q^2 - q^3} - e^{q^3 - q^1}. \quad (49)$$

Here

$$\begin{aligned} P(\mathbf{x}) &= \frac{\partial V}{\partial q^3} - \frac{\partial V}{\partial q^2} = e^{q^1 - q^2} - 2e^{q^2 - q^3} - e^{q^3 - q^1}, \\ Q(\mathbf{x}) &= \frac{\partial V}{\partial q^1} - \frac{\partial V}{\partial q^3} = e^{q^1 - q^2} + e^{q^2 - q^3} + 2e^{q^3 - q^1}, \\ R(\mathbf{x}) &= \frac{\partial V}{\partial q^2} - \frac{\partial V}{\partial q^1} = -2e^{q^1 - q^2} + e^{q^2 - q^3} - e^{q^3 - q^1}, \end{aligned} \quad (50)$$

from which the integrability condition (42) for  $\vec{F} = (P(\mathbf{x}), Q(\mathbf{x}), R(\mathbf{x}))$  can be easily proved, thus concluding that the Toda molecule described by (49) is an integrable dynamical system.

As a generalization, it is interesting to consider the Toda lattice

$$H = \frac{1}{2} \sum_{j=1}^N p_j^2 + \sum_{j=1}^{N-1} e^{(q^{j+1} - q^j)} \quad (51)$$

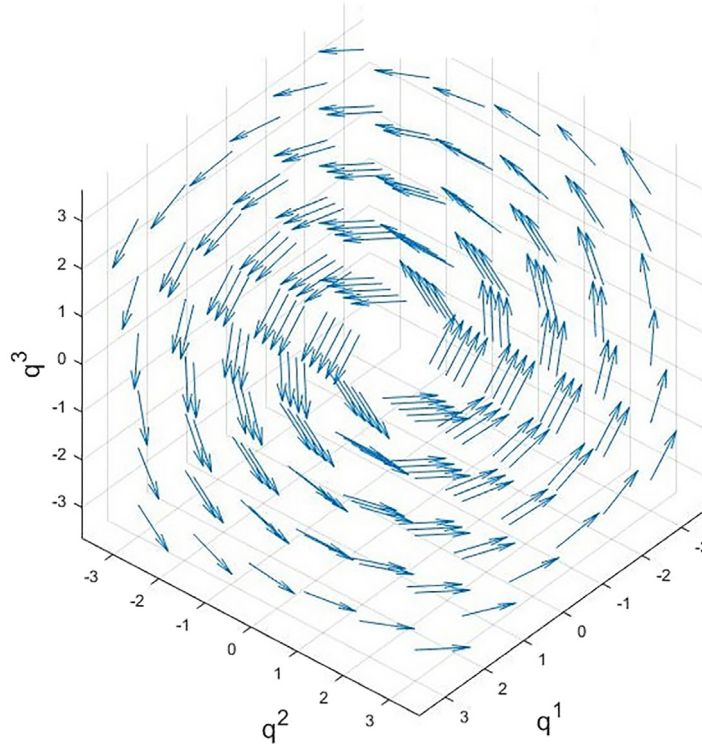


**Fig. 4.** Rotating vector field corresponding to normalized perpendicular vectors to catenary submanifolds for the Kepler problem.

which in the  $N = 3$  case is

$$H = \frac{1}{2} (p_1^2 + p_2^2 + p_3^2) + e^{q^2 - q^1} + e^{q^3 - q^2}, \quad (52)$$

which again fulfills the integrability condition (42). The corresponding normalized vector field, which is perpendicular to the catenary submanifold, is shown in Fig. 5. As can be seen the bundle of catenary submanifolds foliate the configuration space.

### 7.2.3. General Calogero–Moser system

The so-called Calogero–Moser system is described in general by Hamiltonian

$$H = \frac{1}{2} \sum_{j=1}^N (p_j^2 + \omega^2 (q_j^n)^2) + \epsilon^2 \sum_{m,n=1; m \neq n}^N (q^m - q^n)^{-2}. \quad (53)$$

For  $N = 3$  it reads

$$H = \frac{1}{2} (p_1^2 + p_2^2 + p_3^2) + \frac{1}{2} \omega^2 ((q^1)^2 + (q^2)^2 + (q^3)^2) + \epsilon^2 \left[ \frac{1}{(q^1 - q^2)^2} + \frac{1}{(q^1 - q^3)^2} + \frac{1}{(q^2 - q^3)^2} \right]. \quad (54)$$

and it can be confirmed to be integrable for all values of the parameters  $\omega$  and  $\epsilon$ .

### 7.2.4. 3D Choodnovzky system

Our last example of integrable system since fulfilling condition (42) is the 3D Choodnovzky system

$$H = \frac{1}{2} \sum_{j=1}^N p_j^2 + \frac{1}{2} \left( \sum_{j=1}^N (q^j)^2 \right)^2 - \sum_{i=1}^N (q^i)^2 \quad (55)$$

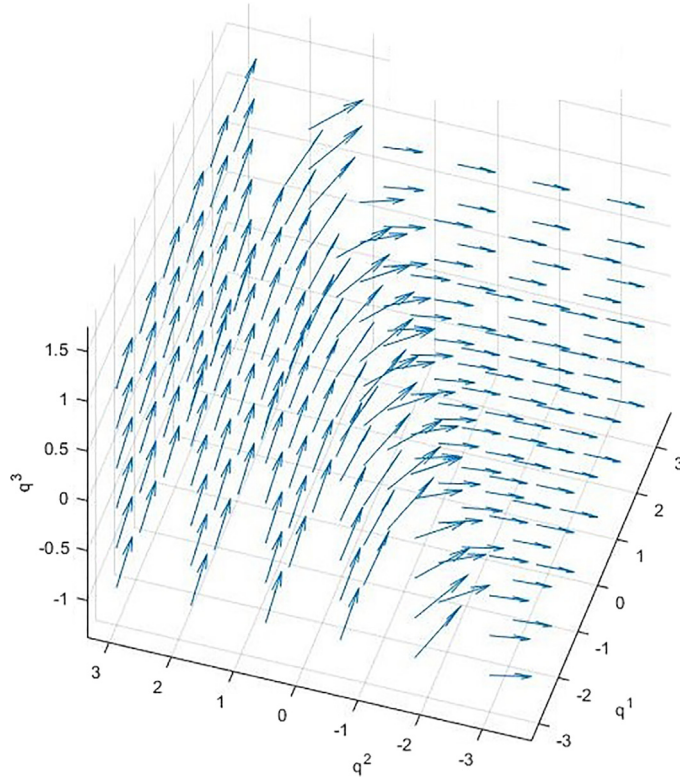


**Fig. 5.** Same as Fig. 4 for the  $N = 3$  Toda lattice.

which for  $N = 3$  reads

$$H = \frac{1}{2} ((p_1)^2 + (p_2)^2 + (p_3)^2) + \frac{1}{2} [(q^1)^2 + (q^2)^2 + (q^3)^2]^2 - [(q^1)^2 + (q^2)^2 + (q^3)^2]. \quad (56)$$

The same happens for the generalized 3D Choodnovzky system, a non-linear fourth degree coupled oscillators with Hamiltonian function

$$H = \frac{1}{2} (p_1^2 + p_2^2 + p_3^2) + \delta_1((q^1)^2 + (q^2)^2 + (q^3)^2) + 2\alpha_2 ((q^2 - q^1)^4 + (q^3 - q^1)^4 + (q^3 - q^2)^4) + \beta_3(q^1 + q^2 + q^3)^4, \quad (57)$$

which is integrable for all values of  $\delta_1, \alpha_2, \beta_3 \in \mathbb{R}$ .

#### 7.2.5. Integrable systems not fulfilling condition (42)

As commented previously (42) is only a sufficiency condition, so that there may exist cases of integrable system not fulfilling it. One such example is

$$H = \frac{1}{2} (p_1^2 + p_2^2 + p_3^2) + [(q^1)^\alpha + (q^2)^\alpha + (q^3)^\alpha], \quad (58)$$

which is obviously integrable since it is separable, but it only fulfills condition (42) for  $\alpha = 0, 1, 2$ .

## 8. Conclusions

We have successfully analyzed the stability regions in the phase space for the Hénon–Heiles 2D system through the *catenary chaos indicator CCI*, introduced by us and generalizing the VWP to Riemannian manifolds.

We proved that this indicator differentiates correctly stable from unstable trajectories in the phase space, and its sensibility is able to detect different levels of stability between trajectories and regions, thus being able to predict the different evolution for each one in the phase space improving the prediction proposed by most indicators.



As shown in the paper the indicator can be applied to dynamical systems in higher dimensions, and particular illustrations are presented for the 3D case.

We have shown that when the previously defined catenary condition is fulfilled along a trajectory locally there is a regular region around this trajectory. We have connected this with Statics through the analogy with David Gregory proposition in arch Structural Mechanics: 'An arch of any form can only be in equilibrium if we can draw a catenary curve which passes through it' (see Fig. 1). From this point of view, we have studied the analogy between catenary curves in Statics and catenary trajectories in Dynamics as stabilizer structures in the configuration space.

Generalizing the previous idea to 3D systems we show that the catenary condition can be understood as a measure of regularity for trajectories, so that applying certain criterion, it is possible to find out a family of 2D *catenary submanifolds* foliating all  $\mathbb{R}^3$  ensuring in this case that the dynamics is regular.

### CRedit authorship contribution statement

**A. Vergel:** Conceptualization, Methodology, Writing, Software, Artwork. **J.C. Losada:** Conceptualization, Methodology. **R.M. Benito:** Conceptualization, Methodology. **F. Borondo:** Conceptualization, Methodology, Writing.

### Declaration of competing interest

The authors declare that they have no known competing financial interests or personal relationships that could have appeared to influence the work reported in this paper.

### Data availability

No data was used for the research described in the article.

### Acknowledgments

This work has been partially supported by the Spanish Ministry of Science and Innovation, Gobierno de España under Contract No. PID2021-122711NB-C21, and by ICMAT Severo Ochoa under Contract CEX2019-000904-S. A.V. gratefully acknowledges support from Margarita Salas Contract No. UP2021-035 financed by the European Union-NextGenerationEU.

### References

- [1] Skokos Ch. In: *Lecture notes in physics*, Vol. 790, 2010, p. 63.
- [2] Skokos Ch, Antonopoulos Ch, Bountis TC, Vrahatis MN. *J Phys A* 2004;37:6269.
- [3] Benítez P, Losada JC, Benito RM, Borondo F. In: Ibáñez S, et al., editors. *Progress and challenges in dynamical systems. Springer proceedings in mathematics & statistics*, Vol. 54, Heidelberg: Springer; 2013, p. 77–88.
- [4] Lega E, Guzzo M, Froeschlé C. *Physica D* 2003;182:179.
- [5] Barrio R. *Chaos Solitons Fractals* 2005;25:711.
- [6] Cincotta PM, Simó C. *Astron Astrophys* 2000;147:205.
- [7] Cincotta PM, Giordano CM, Simó C. *Physica D* 2003;182:151.
- [8] Dumas HS, Laskar J. *Phys Rev Lett* 1993;70.
- [9] Losada JC, Estebaranz JM, Benito RM, Borondo F. *J Chem Phys* 1998;108:63.
- [10] Carmo MP. *Differential geometry of curves and surfaces*. Prentice Hall, Englewood Cliffs; 1976.
- [11] Carmo MP. *Riemannian geometry*. Boston: Birkhauser; 1992.
- [12] Vergel A, Losada JC, Benito RM, Borondo F. *Appl Math* 2014;5:49878.
- [13] Vergel A, Benito RM, Losada JC, Borondo F. *Phys Rev E* 2014;89:022901.
- [14] Vergel A, Montes J, Borondo F. *Phys Rev E* 2022;106:064213.
- [15] Zhu X, Thompson KC, Martínez TJ. *J Chem Phys* 2019;150:164103.
- [16] Yanao T, Koon X, Wang S, Marsden JE. *Phys Rev A* 2006;73:052704.
- [17] Takatsuka H, Teramoto K. *J Chem Phys* 2005;122(7):074101.
- [18] Eisenhart LP. *Ann of Math* 1929;30:591.
- [19] Cipriani P, Bari M. *Phys Rev Lett* 1998;81:5532.
- [20] Casetti L, Clementi C, Pettini M. *Phys Rev E* 1996;54:5969.
- [21] Bari M, Cipriani P. *Planet Space Sci* 1998;46:1543.
- [22] Casetti L, Pettini M, Cohen EGD. *Phys Rep* 2000;337:237–41.
- [23] Cerruti-Sola M, Pettini M. *Phys Rev E* 1995;51:53.
- [24] Cerruti-Sola M, Pettini M. *Phys Rev E* 1996;53:179.
- [25] Di Cairano L, Gori M, Pettini M. *Chaos* 2019;29:123134.
- [26] Horwitz L, Zion YB, Lewkowics M, Schiffer M, Levitan J. *Phys Rev Lett* 2007;98:234301.
- [27] Zion YB, Horwitz L. *Phys Rev E* 2008;78:036209.
- [28] Saa A. *Ann Physics* 2004;314:508.
- [29] Joy MP, Sabir M. *PRAMANA J Phys* 1993;40:17–23.
- [30] Nayfeh AH, Mook DT. *Nonlinear oscillations*. New York: Wiley; 1979.
- [31] Hénon M, Heiles C. *Astron J* 1964;69:73.
- [32] Bernoulli J. *Disquisitio catoptrico-dioptica. Opera Omnia*. Geneve: sumptibus Marci-Michaelis Bousquet & sociorum, I; 1742, p. 369–76.
- [33] Rojo AG. *Amer J Phys* 2005;73:831.
- [34] Meckler A. *Amer J Phys* 1976;44:845–50.

- [35] Quapp W, Heidrich D. Theoret Chim Acta (Berlin) 1984;66:245–60.
- [36] Fukui K. J Phys Chem 1970;74:4161.
- [37] Eyring H, Polanyi M. Z Phys Chem B 1931;12:279.
- [38] Weinan E, Ren W, Vanden-Eijnden E. Phys Rev B 2002;66:052301.
- [39] Weinan E, Weiqing R, Vanden-Eijnden E. J Chem Phys 2007;126:164103.
- [40] Taken from <https://es.wikipedia.org/wiki/Catenaria>.
- [41] Birkhoff GD. C R Acad Sci 1931;192:196.
- [42] Churchill RC, Pecelli G, Rod DL. In: Casati G, Ford J, editors. Stochastic behavior in classical and quantum hamiltonian systems. New York: Springer-Verlag; 1979.
- [43] Arnold VI. Rus Math Surv 1963;18(5):9–36.